Available online at www.sciencedirect.com

jmr&t Journal of Materials Research and Technology

journal homepage: www.elsevier.com/locate/jmrt

Original Article

Towards green synthesis of Mn^{4+}-doped fluoride phosphors: a review☆

Yoon Hwa Kim [a,1], Jungmin Ha [b,1], Won Bin Im [c,*]

[a] Wearable Platform Materials Technology Center, Korea Advanced Institute of Science and Technology (KAIST), 291 Daehak-ro, Yuseong-gu, Daejeon, 34141, Republic of Korea

[b] Materials Science and Engineering Program, University of California, San Diego, 9500 Gilman Drive, Mail Code 0418, La Jolla, CA, 92093, USA

[c] Division of Materials Science and Engineering, Hanyang University, 222 Wangsimni-ro, Seongdung-gu, Seoul, 04763, Republic of Korea

ARTICLE INFO

Article history:
Received 29 June 2020
Accepted 4 January 2021
Available online 8 January 2021

Keywords:
Mn^{4+} emission
Fluoride phosphor
Hydrogen fluoride
Solid-state lighting
HF-free synthesis

ABSTRACT

Mn^{4+}-doped fluoride phosphors are attractive for application in white solid-state lighting devices because their distinct red emission can improve the color rendering index, while the earth-abundance of Mn^{4+} ions can reduce the production cost. However, highly hazardous HF is used as the fluoride source in the synthesis processes, which requires extreme caution. In this review, we introduce various methods for synthesizing Mn^{4+}-doped fluoride phosphors, categorized according to the presence or absence of HF in the synthesis. The underlying optical properties of the phosphors fabricated using the various methods are discussed. In addition, in the discussion of each method, we emphasize on the key factors and strategies for developing phosphors. Finally, this review highlights perspectives on and future directions for the safe synthesis of Mn^{4+}-doped fluoride phosphors to achieve solid-state lighting devices with superior optical properties.

1. Introduction

White solid-state lighting (SSL) devices based on down-converted phosphors with blue light-emitting diodes (LEDs) have become increasingly attractive as light sources, owing to their long lifetimes, production of less toxic waste compared to existing light sources such as incandescent and fluorescent lamps, and their flexible design due to small device sizes [1]. A commercial white LED is fabricated by combining a broad yellow-emitting phosphor, $Y_3Al_5O_{12}:Ce^{3+}$, with a blue LED with an emission spectrum maximum (λ_{em}) of 450 nm. This reduces the production cost and facilitates mass production. However, this method has a critical drawback, namely, a low color quality due to the lack of a red-emitting wavelength region. To overcome this limitation, use of the combination of

☆ This review is dedicated to the memory of Professor Joanna McKittrick, whose activities in the field of luminescent materials and biomaterials have definitely guided us.

* Corresponding author.
E-mail address: imwonbin@hanyang.ac.kr (W.B. Im).

[1] These authors contributed equally.

https://doi.org/10.1016/j.jmrt.2021.01.011

a broad green-emitting phosphor and a broad red-emitting phosphor has been suggested to increase the color rendering index (CRI) of SSL devices, as shown in Fig. 1 [2]. However, this method also presents a limitation, as the device efficiency is reduced because of an overlap between the emission spectrum of the green phosphor and the excitation spectrum of the red phosphor. There is a small overlap between the broad emission spectrum (over 750 nm) of a phosphor mixture with a broad red-emitting phosphor and the human eye sensitivity curve, which drops to zero at 700 nm, thereby resulting in a loss of the remaining emission spectrum. Recently, a phosphor mixture with a narrow red-emitting phosphor has drawn attention, because it prevents reduction in efficiency, owing to the similarity between the excitation regions of the red- and green-emitting phosphors and the convergence with the human eye sensitivity curve. Therefore, the development of narrow red-emitting phosphors is important for obtaining a high CRI and improving the energy efficiency of phosphor-converted white LEDs.

Novel narrow red-emitting phosphors are categorized into three families—the Eu^{2+}-activated nitride phosphor family, perovskite nanocrystal family, and Mn^{4+}-activated fluoride phosphor family [2]. The Eu^{2+}-activated nitride phosphor family is represented by Sr $[LiAl_3N_4]$:Eu^{2+}, which was reported by the Schnick group [3]. The Sr $[LiAl_3N_4]$:Eu^{2+} phosphor has a full-width at half-maximum (FWHM) of approximately 50 nm at an emission spectrum maximum (λ_{em}) of ~654 nm [3]. The sharp red emission arises from the Eu^{2+} ions located in the cuboid or highly symmetrical sites of the nitride host. A large crystal-field splitting (>0.1 eV) between the two highest bands of Eu^{2+} 4*f*-orbitals in the Sr site of the nitride host generates a narrow emission by suppressing overlapping emissions [4]. The optical properties of the Eu^{2+}-activated nitride phosphor family can be controlled by varying the energy difference between the Eu^{2+} ions in novel hosts through manipulation of the nephelauxetic effect, crystal-field splitting, and the Stokes shift, among other factors. Recently, the Sr $[Li_2Al_2O_2N_2]$:Eu^{2+} phosphor with a narrow FWHM (~48 nm) for λ_{em} centered at 614 nm was investigated for achieving higher luminous efficacy than commercial high color-rendering phosphor-converted white LEDs [5]. These phosphors are usually synthesized through a high-temperature solid-state reaction under a reducing atmosphere and high-pressure conditions. In addition, due to their moisture sensitivity, these nitride hosts must be carefully kept in dry storage.

The perovskite nanocrystal family represented by $CsPbX_3$ (X = Cl, Br, and I) exhibits FWHM values in the range of 12–42 nm [6]. Kovalenko et al. reported colloidal synthesis of monodisperse $CsPbX_3$ nanocrystals using hot injection [7]. The sharp red emission of $CsPbI_3$ originates from the band-to-band transition of excitons from the conduction band, formed by the overlap of Pb *p*-orbitals, to the valence band, formed by the overlap of halide *p*-orbitals. These nanocrystals have a higher photoluminescence quantum yield and a narrower FWHM than other red phosphors. To tune the optical properties of this nanocrystal family, the anion I^- is exchanged with Br^-, or the cation sites, Cs^+ and Pb^{2+}, are substituted with other ions. However, this family has toxicity issues due to the Pb^{2+} ions in the host, in addition to stability issues related to the host.

Mn^{4+}-doped fluoride phosphors were reported by Adachi et al. and General Electronics (USA), with an FWHM of approximately 50 nm and an emission spectrum with sharp peaks. These sharp peaks can be attributed to the $3d^3$–$3d^3$ transitions from electric–dipole–forbidden transitions ($^2E_g \rightarrow {}^4A_{2g}$) in the octahedral site $[MnF]^{6-}$ of A_2MF_6 (A = Na, K, or Cs and M = Si, Ti, Ge, or Zr), where the transitions of the Mn^{4+} ions in the octahedral sites are specified by the value of the crystal field parameter. Therefore, the optical properties can be determined from the type of host, which possesses octahedral sites for Mn^{4+} ion substitution. The fluoride phosphor family can also increase the color quality by enhancing the zero-phonon line (ZPL) emission of Mn^{4+} ions. Fluoride phosphors are usually synthesized using HF. This family has received significant attention because it is relatively easy to scale-up the fabrication of phosphor and white LEDs. However, when used in the synthesis process, HF needs to be handled with extreme caution because of its high toxicity. Thus, many researchers have concentrated on developing HF-free synthesis methods for fluoride phosphors. Current reviews focus on the synthesis methods of fluoride phosphors [8–10], but a summary of synthesis methods regarding the presence or absence of HF has not been reported.

In this review, the relevant synthesis methods are classified into two categories, namely those with and without the use of HF. The former includes etching, co-crystallization,

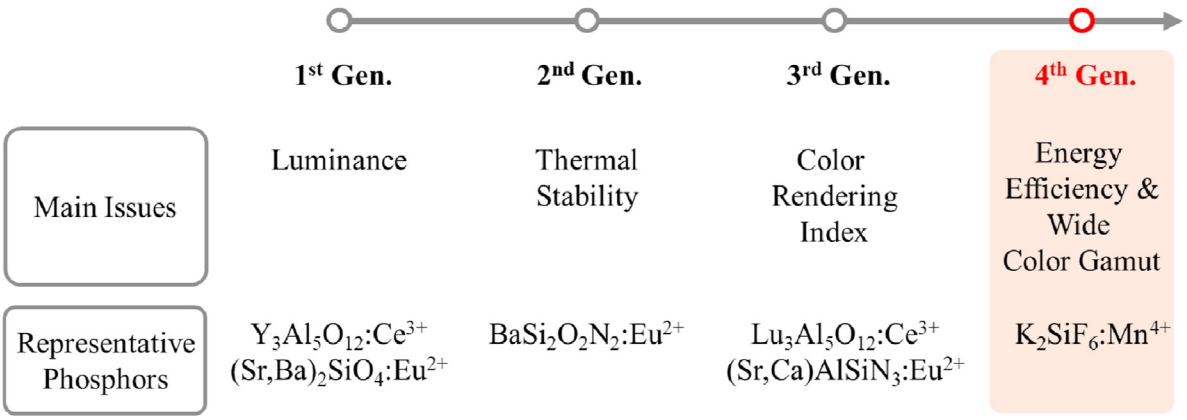

Fig. 1 – Development scheme of phosphors for phosphor-converted white LEDs. Modified from ref. [2].

hydrothermal, and co-precipitation methods, while the latter comprises the co-precipitation/sol–gel method with low toxicity acids and the microwave/ionothermal method with ionic liquids. Moreover, HF-free methods with commercial K_2MnF_6 as an Mn^{4+} ion source are presented. Finally, this review provides perspectives and future directions for the synthesis of Mn^{4+}-doped fluoride phosphors with respect to safety and achieving superior optical properties.

2. Basics of Mn^{4+}-doped fluoride phosphors

2.1. *Luminescent mechanism of Mn^{4+} ions in fluoride phosphors*

Mn^{4+} has three electrons in the unfilled 3*d*-orbital of the outer shell. These electrons are thus sensitive to the crystal environment. Under the local crystal field environment, the five degenerate *d*-orbitals ($d_{x^2-y^2}$, d_{xy}, d_{z^2}, d_{xz}, *and* d_{yz}) split into the doubly-degenerate e_g and triply-degenerate t_{2g} orbitals. The distance between e_g and t_{2g} is denoted as 10 Dq, which is a parameter for characterizing the field strength.

The Tanabe–Sugano (T–S) diagram (Fig. 2) shows the relationship between the energy levels of Mn^{4+} (E/B) and the crystal field strength (Dq/B) of the $3d^3$ configuration in an octahedral crystal field, where B is the Racah parameter used to describe the effects of electron–electron repulsion within the metal complex [11,12]. The T–S diagram aids in the identification of each emission peak in relation to the energy levels of transition metal ions. It is clearly shown that the energies of the multiplets have a strong dependence on the crystal field strength except for the $2T_{1g}$ and $2E_g$ levels. In the diagram, the emission spectra arise from the $^2E_g \rightarrow {}^4A_{2g}$ transition (sharp peaks) [13] while the two measured broad excitation bands mainly originate from the $^4A_{2g} \rightarrow {}^4T_{1g}$ and $^4A_{2g} \rightarrow {}^4T_{2g}$ spin-allowed transitions (Fig. 2) [12].

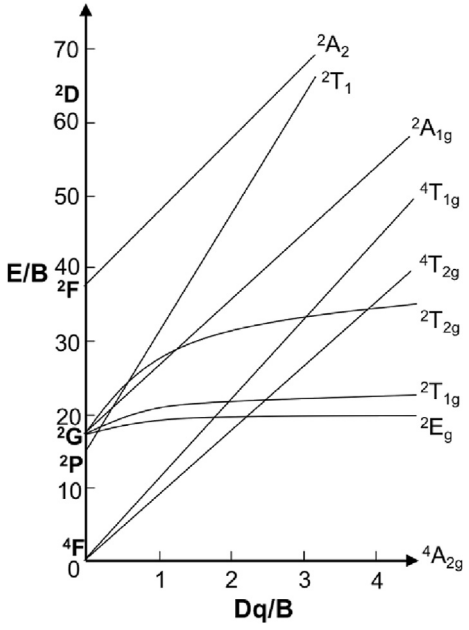

Fig. 2 – Tanabe–Sugano energy diagram of the $3d^3$ configuration in an octahedral crystal field. Adopted and reproduced with permission from Ref. [12], copyright 2014, Elsevier.

The Mn^{4+}-activated fluorides are representative of red-emitting fluoride phosphors [14–20]. The narrow-band red emission of Mn^{4+} in fluorides is attributed to the $^2E_g \rightarrow {}^4A_{2g}$ transition that consists of emission peaks from the ν_3 (t_{1u}), ν_4 (t_{1u}), and ν_6 (t_{2u}) (anti-Stoke emissions), ZPL, and ν_6 (t_{2u}), ν_4 (t_{1u}), and ν_3 (t_{1u}) (Stokes emissions) vibronic modes of the octahedral group $[MnF_6]^{2-}$ [15,19–23]. The location of the ZPL depends on the constituent elements, composition, and host lattice structure [19].

2.2. *Host for Mn^{4+}-doped fluoride phosphors*

The host, which includes F, can be classified into four different groups that possess substitution sites for Mn^{4+} ions—(1) fluoride, (2) oxyfluoride, (3) hydroxy and hydrate fluoride, and (4) alkali bifluoride-based compounds. The fluoride-based group consists of A_2XF_6, A_3XF_7, $BaXF_6$, and A_3ZF_6 (A = monovalent ions such as Na, K, Cs, Rb, and NH_4, X = Si, Ti, Hf, Zn, Sn, etc., Z = trivalent ions such as Sc, Gd, and Al), and the compositions in this group only have F anion substitution sites. A_2XF_6 is represented by K_2SiF_6 and is treated as the basic structure in this review. The oxyfluoride-based group consists of $3.5MgO{\cdot}0.5MgF_2{\cdot}GeO_2$, A_2NbOF_5 (A = Cs and Rb), $A_2WO_2F_4$ (A = Cs and Na), etc. Adachi et al. further sub-divided the fluoride and oxyfluoride groups into two groups with respect to the difference in photoluminescence (PL) spectral features by observing the ZPL emission at room temperature [24]. For example, the wavelength of ZPL emission is the same (~622 nm) for Mn^{4+}-activated K_2TiF_6, K_2GeMnF_6, and K_2SiMnF_6, despite the differences in constituent elements. Anti-Stokes emissions are located in a shorter wavelength range with respect to the ZPL, at ~598 nm, ~607 nm, and ~610 nm; Stokes emissions occur at a longer wavelength range at ~632 nm, ~635 nm, and ~645 nm for K_2XF_6 (X = Ti, Ge, Si) [19]. In contrast, the ZPL emission for $Na_2SiF_6{:}Mn^{4+}$ is observed at ~617 nm, and the three anti-Stokes and Stokes emissions are blue-shifted compared to those for $K_2XF_6{:}Mn^{4+}$. This demonstrates that the substitution of the A element influences the ^2E_g energy level of Mn^{4+} more than the substitution of the X element [19], which is corroborated by previous studies [15,25]. The decrease in the energy of the ^2E_g level has been attributed to a decrease in the radius or electron affinity of the A element [15,19,25,26]. However, this has not been proven theoretically and requires further study. The hydroxy and hydrate fluoride-based group comprises the compounds $BaNb(OH)_{1.5}F_{5.5}$, $ZnSiF_6{\cdot}6H_2O$, and $K_2SnF_6{\cdot}H_2O$, while the alkali bifluoride-based group includes $NaHF_2$, which has octahedral sites through fluoride ion formation.

3. Synthesis methods involving the use of HF

3.1. *Etching*

Adachi et al. synthesized a $K_2SiF_6{:}Mn^{4+}$ phosphor by means of wet chemical etching of a Si wafer [14]. This method uses an

etching target and an etchant containing HF, $KMnO_4$, and deionized water at room temperature without stirring. HF affects the F^- ions by prohibiting the oxidation and hydrolysis of F, and it also prevents the reduction of Mn^{4+} ions (Fig. 3a). The yellowish powder displayed in Fig. 3b, namely $K_2SiF_6:Mn^{4+}$, was produced after completion of the synthesis through the following chemical reaction (Eqn (1)) [14]:

$$Si + 4KMnO_4 + 12HF \rightarrow K_2SiF_6 + K_2MnF_6 + 3MnO_2 + 6H_2O + 2O_2 \quad (1)$$

A sharp emission centered at 630 nm was observed in $K_2SiF_6:Mn^{4+}$, which is caused by the conventional Mn^{4+} emission in the $[SiF_6]^{2-}$ octahedral site of the K_2SiF_6 host [27]. This method suggests that the etching target for the X site and the etchant for the A site can be altered to synthesize various A_2XF_6 hexafluoride compositions (A = Na, K, Cs, NH_4, etc.; X = Si, Ti, Ge, etc.). K_2SiF_6, Na_2SiF_6, and Na_2GeF_6 were produced using this method [15]. $NaMnO_4$ was used as an oxidizing agent in the HF/H_2O solution instead of $KMnO_4$ to substitute Na into the host, and Ge shots were included to prepare the $Na_2GeF_6:Mn^{4+}$ phosphor. Si powder was obtained from crushed quartz [28] to reduce the cost, and other glass powders, such as fused quartz, borosilicate, and soda-lime glass [29], have also been used as an alternative Si source instead of expensive Si wafers. The $K_2SiF_6:Mn^{4+}$ phosphor synthesized from crushed quartz showed a weaker PL emission than that from a single crystalline Si wafer due to the porous-like structure of the crushed quartz. In contrast, the use of glass powders (fused quartz, borosilicate, and soda-lime glass) as the Si source for the wet etching method resulted in single-phase K_2SiF_6 and optical properties similar to those of the single-crystalline Si wafer [29].

The particle size of the fluoride phosphor obtained from the wet chemical etching method was irregular. To obtain a regular particle size, a pulsed laser irradiation method was combined with the chemical etching method [30]. In this modified method, as-prepared $K_2SiF_6:Mn^{4+}$ phosphor prepared by wet chemical etching was dispersed in a methanol solvent in a quartz cuvette, and then, a pulsed laser light was irradiated into the solution for 6 h with continuous stirring. To prevent undesired effects, the laser beam was defocused by placing the focus just ahead of the cuvette. Laser wavelengths of 532, 355, and 266 nm were chosen to observe the change in particle size with respect to the irradiation power. The mean diameter, D_{mean}, of the particles decreased with increasing irradiation energy (D_{mean} = 2.7, 3.5, and 4.7 μm for wavelengths of 266, 355, and 532 nm, respectively), as confirmed using scanning electron microscopy. However, the PL quantum efficiency (QE) of the phosphors decreased after irradiation, which might be due to defects such as fragmentation-induced strain and/or cracks.

Although the etching method does not require high temperatures, this method still involves challenges, such as the high cost of pure Si or metal for the etching target, the low product yield of phosphors due to the MnO_2 impurity phase resulting from high $KMnO_4$ concentrations, and the need for precise control to obtain a narrow particle distribution.

3.2. *Co-crystallization*

The preparation of hexafluoride materials is performed through the crystallization of a mixture of a HF solution with an alkali metal fluoride and an X site precursor (oxide or metal form) to form K_2XF_6 at room temperature. The crystals react with the HF solution, containing $[MnF_6]^{2-}$ ions from K_2MnF_6, and then, hexafluoride phosphor is synthesized through co-crystallization [31]. Setlur et al. reported a potential $K_2TiF_6:Mn^{4+}$ and $K_2SiF_6:Mn^{4+}$ phosphor synthesis method based on co-crystallization for application in white LEDs. The synthesized $K_2TiF_6:Mn^{4+}$ and $K_2SiF_6:Mn^{4+}$ phosphors exhibit high efficiencies and high CRIs by combining an InGaN blue LED and a yellow-green phosphor [32]. In this synthesis process, the host fluoride and K_2MnF_6 were dissolved in a 70% HF solution with a Mn^{4+} concentration ranging from 3 to 8%; this process is called Bode's method. The obtained powders were dry-milled to obtain a median particle size in the range of 15–20 μm. However, this method is not suitable for mass production because of the difficulty in controlling the reaction time and the need for a large quantity of toxic HF.

3.3. *Hydrothermal method*

The hydrothermal method typically requires high temperatures and high vapor pressure for crystallizing materials from aqueous solutions. Two types of hydrothermal methods are

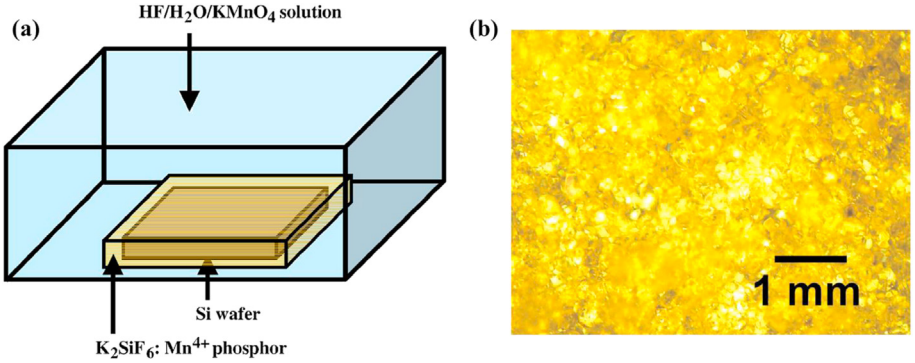

Fig. 3 – (a) Chemical etching of the Si wafer in a $HF/H_2O/KMnO_4$ solution for synthesizing $K_2SiF_6:Mn^{4+}$ phosphor. (b) Optical microscopic view of the chemically synthesized $K_2SiF_6:Mn^{4+}$ phosphor on the Si(100) wafer. Reproduced with permission from Ref. [14], copyright 2008, American Institute of Physics.

used for synthesizing fluoride phosphors. One is the two-step method, where the phosphor host is initially obtained using a hydrothermal method, and then, the Mn source is obtained through another method such as precipitation. The other is the direct hydrothermal method (one-pot hydrothermal process).

In the two-step hydrothermal method, the hydrothermal method is used in the first step to synthesize the phosphor host, while the second step is the substitution process, wherein the host is dipped in a HF solution with $KMnO_4$. Since the oxidation or reduction of Mn^{4+} occurs easily when only the hydrothermal process is performed, the Mn^{4+} source is prepared separately. Hexafluoride phosphors [33–41], $K_2MF_7:Mn^{4+}$ [42], $KNaMF_7:Mn^{4+}$ (M = Nb and Ta) [43], $K_3TaO_2F_4:Mn^{4+}$ [44], and $BaTiOF_4:Mn^{4+}$ [45] were synthesized through this two-step method. The controlling factors involved in optimizing the characteristics of the phosphor are the temperature, reaction time, host precursors, and concentration of raw materials. For example, $BaGeF_6:Mn^{4+}$ phosphors were synthesized from $BaCO_3$, GeO_2, and $KMnO_4$ in a HF solution by controlling the HF and $KMnO_4$ concentrations, as well as the synthesis temperature (Fig. 4a) [36,46]. An increase in the HF concentration from 10% to 40% (v/v) continuously enhanced the PL intensity because a higher HF concentration is beneficial for the formation of the stable $[MnF_6]^{2-}$ group. To obtain the highest PL intensity, $KMnO_4$ was added at concentrations ranging from 0 to 14 mmol L^{-1} and the highest PL intensity was observed at 10 mmol L^{-1}, while the reaction temperature was controlled from 25 to 180 °C. As shown in Fig. 4b, $BaGeF_6:Mn^{4+}$ phosphors synthesized at different reaction temperatures produced a single phase of $BaGeF_6$ crystals. The PL intensities were enhanced with the increase in the reaction temperature up to 100 °C, and then, the emission intensity decreased with temperatures above 100 °C due to aggregation in the morphology, as shown in Fig. 4c. The sample synthesized at 25 °C exhibited a rod-like shape, and its morphology changed to a flower-like shape upon increasing the reaction temperature. At temperatures higher than 140 °C, rod-like particles appeared with an increased average length (Fig. 4d). $BaGe_{1-x}Ti_xF_6:Mn^{4+}$ solid-solution phosphors were also reported, with TiO_2 as the Ti source [47]. Nitrates and organic compounds were used as precursors to prepare single-phase phosphors, and the final product showed a uniform morphology similar to that obtained using the etching method [33,36].

The one-step hydrothermal method is performed directly using raw precursors for a host, including the Mn source and HF solution. Hexafluoride [46,48–53] was synthesized using this method, in which the reduction condition of the Mn source is important for obtaining high-quality phosphors. $KMnO_4$ is used as the main source of Mn since the Mn^{7+} ions in $KMnO_4$ are reduced under acidic conditions. The HF-affected $BaSiF_6:Mn^{4+}$ phosphor was produced using the one-step hydrothermal method using BaF_2 [49], $BaCO_3$ [51], or $Ba(NO_3)_2$ [50,52] as the Ba source and H_2SiF_6 [49] or $(NH_4)_2SiF_6$ [50] as the Si and F sources in the HF and $KMnO_4$ mixed solutions. These

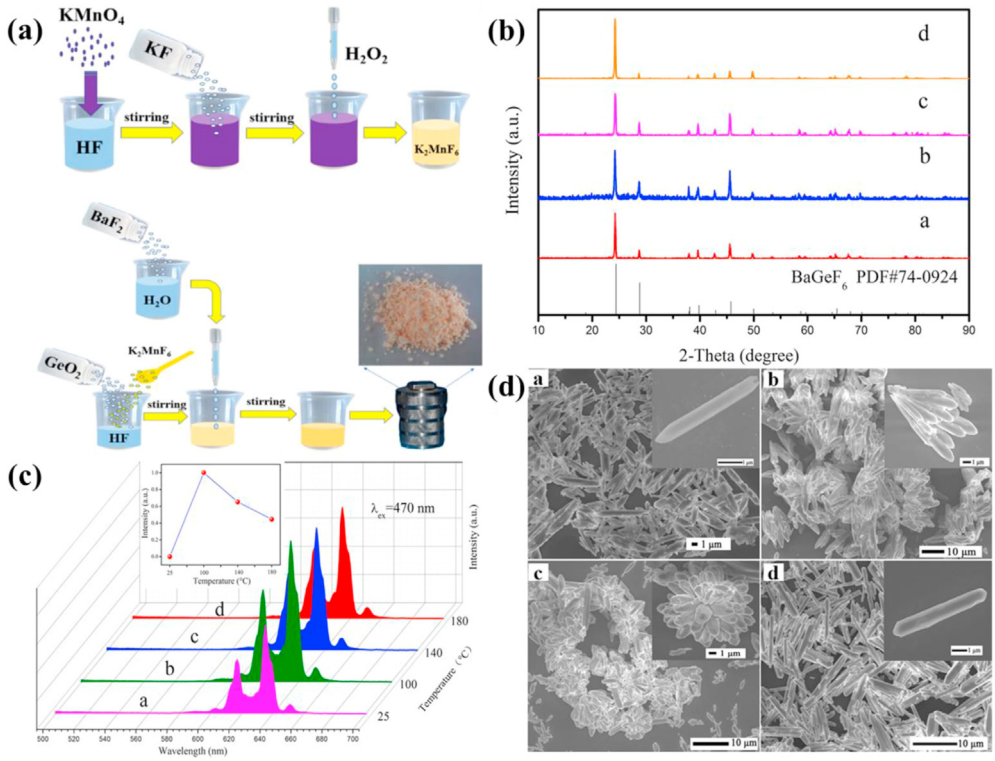

Fig. 4 – (a) Diagram of the experimental process for synthesizing $BaGeF_6:Mn^{4+}$ products. (b) XRD patterns, (c) emission spectra, and (d) SEM images of $BaGeF_6$:2%Mn^{4+} synthesized at different reaction temperatures for 8 h (Inset): The corresponding integrated emission intensity of $BaGeF_6$:2%Mn^{4+} as a function of reaction temperature. a-25, b-100, c-140, and d-180 °C. Reproduced with permission from Ref. [36], copyright 2018, American Chemical Society.

precursors can be replaced with fluorides, carbonates, oxides, metallic forms, etc. For the Si source, when $BaSiF_6:Mn^{4+}$ phosphors are synthesized using Si metal and SiO_2 powder, the phosphor from the Si metal has better crystallinity than that from the SiO_2 powder [49]. Accordingly, the phosphor from Si metal exhibits a higher PL intensity than that from the SiO_2 powder. Similar to the etching method mentioned previously, the hydrothermal method using Si metal for the Si source also has a lower phosphor yield.

The hydrothermal method has a higher yield of synthesized phosphor, while a much lower concentration of $KMnO_4$ is used compared to the etching method. However, this method requires a working temperature of over 100 °C and high pressures along with using the HF solution. It is also difficult to obtain uniform particle sizes, which can affect the optical properties due to etching by HF.

3.4. *Co-precipitation*

The co-precipitation method is composed of two steps. The first step is the preparation of K_2MnF_6, and the second one is the preparation of a Mn^{4+}-doped fluoride phosphor from the combination of cation sources and the K_2MnF_6 obtained from the first step in the HF solution. Since Liu and Chen et al. reported the synthesis of $K_2TiF_6:Mn^{4+}$ phosphor using co-precipitation [17], this method has been used to synthesize various fluoride phosphors because the method of reducing Mn^{4+} ions is comparatively simpler than the other methods [39,54–66]. Moreover, co-precipitation is preferred because it is efficient and more cost-effective than the etching method. To optimize the optical properties, the reaction temperature, reaction time, HF concentration, and quantity of K_2MnF_6 can be controlled, as in the previous methods.

Furthermore, a solvent can be used to enhance the optical properties by controlling the morphology of the phosphor. Liu et al. studied the ultra-fast self-crystallization of the $K_2GeF_6:Mn^{4+}$ phosphor based on the good–poor solvent strategy [64]. The hosts, K_2GeF_6 and K_2MnF_6, were dissolved in a HF solution, which served as a good solvent, and then, ethanol was added as the poor solvent (Fig. 5a). After these reactions, a bright yellow powder was produced instantly, as displayed in Fig. 5b. Ethanol was added in controlled amounts of 5, 10, and 25 mL (hereafter referred to as R1, R2, and R5, respectively.) The X-ray diffraction (XRD) results show that the phosphor phase changes from $P\bar{3}m1$ to $P6_3mc$ with an increasing amount of ethanol (Fig. 5c). The R1 sample, corresponding to the $P\bar{3}m1$ phase, had an octahedral shape with a particle size of ~20 μm, while the R5 sample had a relatively smaller particle size of ~0.6 μm (Fig. 5d, e). The R2 and R5 samples contained the $P6_3mc$ phase, which was unstable relative to the $P\bar{3}m1$ phase of the K_2GeF_6 structure. Additionally, the R1 sample showed a

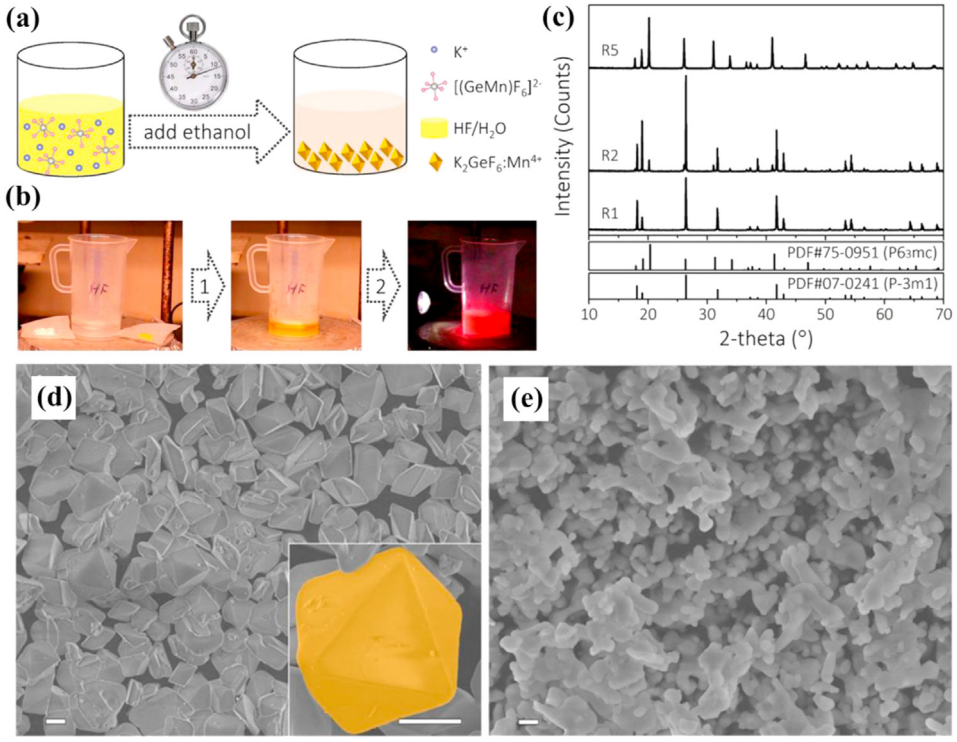

Fig. 5 – (a) Schematic diagram of good–poor solvent strategy for the fabrication of the $K_2GeF_6:Mn^{4+}$ phosphor. (b) Images of three key states during the fabrication process: (1) K_2GeF_6 and K_2MnF_6 powders are dissolved in HF to form a yellow transparent solution; (2) addition of ethanol causes ultrafast self-crystallization of $K_2GeF_6:Mn^{4+}$, which emits intense red light under light radiation at 460 nm. (c) XRD patterns of the $K_2GeF_6:Mn^{4+}$ products and SEM images of (d) R1 and (e) R5 samples; the scale bars are (d) 10 μm and (e) 1 μm, respectively. Reproduced with permission from Ref. [64], copyright 2018, American Chemical Society.

sharp red emission peak arising from Mn^{4+} ions, and the optimized sample exhibited a high internal QE (93%).

Another phosphor, two-dimensional (2D) $K_2TiF_6:Mn^{4+}$, was produced via alcohol-assisted co-precipitation using a HF solution with a mixture of KHF_2, $Ti[OCH(CH_3)_3]_4$, and K_2MnF_6 [67]. 1-propanol was added to the HF solution, which was worked as guidance for growing the 2D morphology of the $K_2TiF_6:Mn^{4+}$ phosphor and this mechanism was confirmed by density functional theory calculations. Other alcohols, such as methanol, 1-butanol, tert-butanol, and 1-pentanol, were also used to build the 2D morphology. These results indicate that the synthesis rate can be accelerated and the morphology of fluoride phosphors improved by adding a solvent in the synthesis process.

3.5. *Other methods*

Beyond the aforementioned methods, other methods have rarely been researched. Zhang et al. reported the synthesis of a $K_2TiF_6:Mn^{4+}$ phosphor using the ball-milling process [68]. The slurry was prepared using K_2TiF_6 powders as a phosphor host and $KMnO_4$ as the Mn source in a HF solution. They controlled the speed of the ball-milling at 100 and 200 rpm for the reaction. The optimized condition (100 rpm) produced K_2TiF_6 with no impurities, but a faster ball-milling speed (200 rpm) produced K_2TiF_6 with K_2MnF_6 as the impurity. The particle size of the phosphor decreased with an increase in the ball-milling speed. In contrast, the Mn concentration increased with an increase in the ball-milling speed. This report explained that an increase in the speed of the ball-milling process increases the surface area and surface energy of the particles, contributing to high Mn^{4+} doping in K_2TiF_6. However, this results in the formation of excessive defects and high Mn concentrations, thereby reducing the optical properties.

In this section, we introduced various methods involving the use of HF for synthesizing fluoride phosphors. These methods, summarized in Table 1, produce fluoride phosphors with high efficiency because of the presence of HF. The role played by HF is to reduce the Mn^{4+} ions by providing an acidic condition. It also supplies sufficient F^- ions to prevent the oxidation of Mn^{4+} ions and to maintain the $[MnF_6]^{2-}$ ion group. However, HF is highly hazardous, so it must be handled with the greatest care to avoid exposure. Therefore, HF-free synthesis methods have been investigated for reasons of health and safety, and these are discussed in the following section.

4. Synthesis methods without the use of HF

4.1. *Hydrothermal method using a low toxicity acid*

As mentioned in the previous section, HF has a high toxicity. Therefore, to avoid the use of HF, Huang et al. developed a new green hydrothermal synthetic method to synthesize red-emitting $K_2SiF_6:Mn^{4+}$ phosphor by using low toxicity H_3PO_4/KHF_2 instead of the toxic HF liquid [69]. The synthetic process is shown in Fig. 6. It involves the following two steps— (1) preparation of soluble manganese (IV) $[Mn(H_3PO_4)_2]$ and (2) hydrothermal synthesis of $K_2Si_{1-x}F_6:xMn^{4+}$ (KSFM) with SiO_2, KHF_2, and $Mn(H_3PO_4)_2$. In step (1), $KMnO_4$ was dissolved in a $CH_2O_2{\cdot}K$ solution using ultrasonic vibration to form active $MnO(OH)_2$. The dark brown $MnO(OH)_2$ solid, after collection by centrifugation and washing, was added to the phosphoric acid with ultrasonic vibration to prepare the $Mn(H_3PO_4)_2$ solution. In step (2), SiO_2 and KHF_2 were mixed in the $Mn(H_3PO_4)_2$ solution and placed in a Teflon cup. The ratio of SiO_2:KHF_2 was varied from 1:3 to 1:30 (Si:F = 1:6–1:60) to optimize the synthesis conditions. The Teflon cup was sealed in an autoclave and kept at 180 °C for 6 h, and the final product was obtained by centrifugation, washing in distilled water, and drying under a vacuum at 40 °C for 24 h.

Fig. 7 shows the XRD patterns, normalized integrated emission intensity, and photographs of KSFM according to the Si:F atomic ratios (1:6–1:60). The XRD patterns did not show any changes, despite the changes in the Si:F ratios, as shown in Fig. 7a. However, the emission intensity increased (Fig. 7b) when the Si:F ratio was changed from 1:6 (sample A) to 1:48 (sample G) and then decreased at 1:60 (sample H). This indicates that an excessive quantity of F does not influence the crystal structure or produce impurities. This result was further confirmed using energy dispersive spectrometry, where the atomic ratio of K:Si:F was found to be 19:8:71 for samples A–H. This study explained that the concentration of F^- plays a key role in controlling the actual concentration of Mn^{4+}, which was analyzed using electron paramagnetic resonance spectroscopy. The absorption value of Mn^{4+} increased from Si:F = 1:6 to the maximum value at Si:F = 1:48, and then decreased at Si:F = 1:60, which corresponded to the PL emission intensity. These results suggest that the red emission of $K_2SiF_6:Mn^{4+}$ is controlled by the concentration of F^-, provided by KHF_2, due to the change in the activator Mn^{4+} concentration in $K_2SiF_6:Mn^{4+}$. The photographs of the synthesized KSFM (Fig. 7c) are in accordance with the results of the PL analysis.

As previously mentioned, the oxidation or reduction of Mn^{4+} occurs rapidly if the HF concentration is insufficient. H_3PO_4/KHF_2 plays an important role in protecting Mn^{4+} from oxidation or reduction. $Mn(H_3PO_4)_2$ is formed by reacting $KMnO_4$ with $CH_2O_2{\cdot}K$ and phosphoric acid, as expressed in Eqs (2) and (3):

$$2MnO_4^-(aq) + 3CHO_2^-(aq) + 3H_2O(l) \rightarrow 2MnO(OH)_2(s) + 3CO_2(g) + 5OH^-(aq) \quad (2)$$

$$2MnO(OH)_2(s) + 2H_2L(aq) \rightarrow MnL_2(aq) + 3H_2O(l) \text{ where } L = H_3PO_4 \quad (3)$$

MnL_2 is slowly changed to $[MnF_6]^{2-}$, and SiO_2 is converted into $[SiF_6]^{2-}$ in the H_3PO_4 solution when KHF_2 is added, as expressed by Eqs (4) and (5). $K_2Si_{1-x}Mn_xF_6$ (s) is produced immediately after $[MnF_6]^{2-}$ and $[SiF_6]^{2-}$ are formed, as shown in Eqn (6).

Table 1 – Summary of synthesis methods using HF for Mn^{4+}-doped fluoride phosphors.

Methods	Synthesis conditions	Advantage	Disadvantage	Host	Reference
Etching	Room temp.	• Does not require high temperatures • Products with high quantum efficiency	• Toxic synthesis conditions due to HF • High cost of Si or metal for etching targets • Low product yield • Necessary to control particle distributions	A_2XF_6 hexafluoride compositions (A = Na, K, Cs, NH_4, etc.; X = Si, Ti, Ge, etc.)	[14,15,27–30]
Co-crystallization	Room temp.	• Does not require high temperatures	• Toxic synthesis conditions due to HF • Difficult to control the reaction time • Large amount of HF is needed	K_2SiF_6 K_2TiF_6	[31,32]
Hydrothermal method	High temperature (<250 °C) with high vapor pressure	• Synthesis of various compositions • High product yield	• Toxic synthesis conditions due to HF • Necessity of high temperature and pressure in synthesis • Difficult to control the particle distributions	A_2XF_6 hexafluoride compositions K_2MF_7 $KNaMF_7$ (M = Nb and Ta) $K_3TaO_2F_4$ $BaTiOF_4$ tetrafluoride	[33–53]
Co-precipitation	$-16\ °C < T \leq 100\ °C$	• Does not require high temperatures • Synthesis of various compositions • More cost-effective than other methods	• Toxic synthesis conditions due to HF	A_2XF_6 hexafluoride compositions (A = Na, K, Cs, NH_4, etc.; X = Si, Ti, Ge, etc.)	[17,39,54–67]
Ball-milling	Room temp.	• Does not require high temperatures	• Toxic synthesis conditions due to HF • Reduction of optical properties	K_2TiF_6	[68]

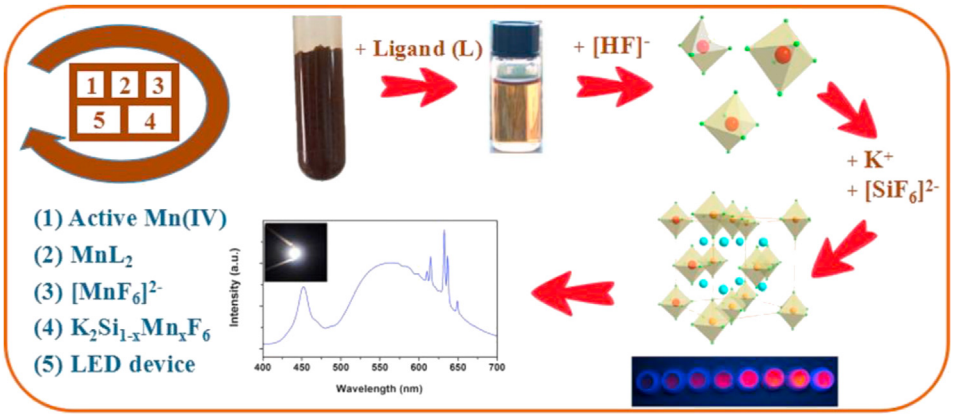

Fig. 6 – $K_2SiF_6:Mn^{4+}$ synthetic route using H_3PO_4/KHF_2. Reproduced with permission from Ref. [69], copyright 2016, American Chemical Society.

$$MnL_2(aq) + 3[HF_2]^-(aq) + H^+(aq) \leftrightarrow [MnF_6]^{2-}(aq) + 2H_2L(aq), \text{ where } L = H_3PO_4 \quad (4)$$

$$SiO_2(s) + 3[HF_2]^-(aq) + H^+(aq) \rightarrow [SiF_6]^{2-}(aq) + 2H_2O(aq) \quad (5)$$

$$2K^+(aq) + (1-x)[SiF_6]^{2-}(aq) + x[MnF_6]^{2-}(aq) \leftrightarrow K_2Si_{1-x}Mn_xF_6(s) \quad (6)$$

During these processes, H_3PO_4/KHF_2 plays a crucial role in stabilizing Mn^{4+} and preparing $[MnF_6]^{2-}$. However, the reported QE was only 28% in this work, which is much smaller than the reported QE (74%) of the compound synthesized with a HF solution [9,70]. This work shows the potential to replace toxic HF in the preparation of Mn^{4+} fluoride phosphors, but it remains challenging to prepare phosphors with high QEs.

4.2. *Microwave synthesis using ionic liquids*

The use of an ionic liquid is another method suitable for the synthesis of fluorides without the use of toxic HF [71–74]. An ionic liquid is defined as an organic salt that typically has a melting temperature of <100 °C and can act as both a solvent and a reactant [75,76]. This organic component is asymmetric and large, providing a low melting temperature. Olchowka et al. [71] reported a microwave radiation synthesis method for A_2SiF_6 (A = Li, Na, K, Rb, and Cs) with an ionic liquid, 1-butyl-3-methylimidazolium hexafluorophosphate ([Bmim]PF_6) as the solvent, and F^- as the precursor. Fig. 8a illustrates that [Bmim]PF_6 decomposes at a temperature of 140 °C to release F^- ($PF_6^- \rightarrow PF_5 + F^-$). Base on this decomposition, [Bmim]PF_6 is used as a F^- precursor in place of HF to synthesize A_2SiF_6. It was confirmed through XRD analysis (Fig. 8b) that the compounds A_2SiF_6 were successfully synthesized. This report demonstrated the possibility of synthesizing

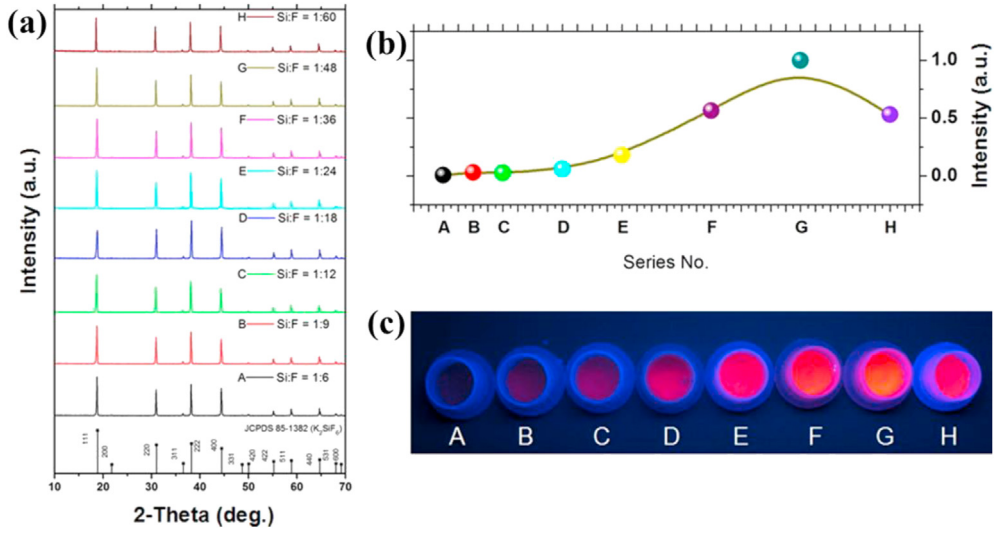

Fig. 7 – (a) X-ray diffraction patterns, (b) normalized integrated emission intensity, and (c) photographs of $K_2SiF_6:Mn^{4+}$ according to the ratio Si:F = 1:6–1:60. Reproduced with permission from Ref. [69], copyright 2016, American Chemical Society.

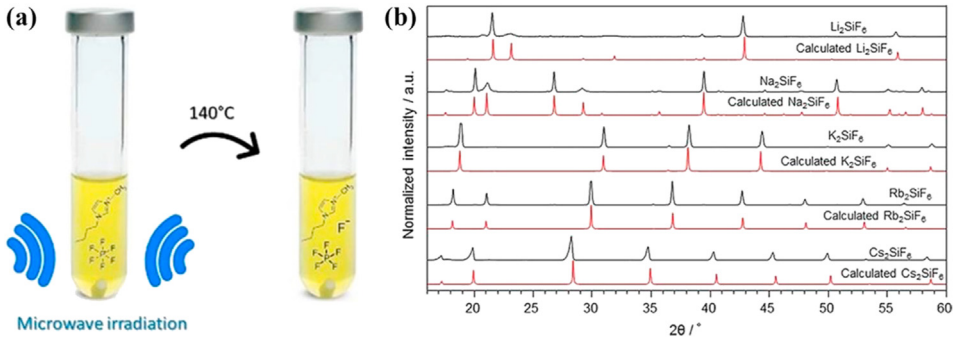

Fig. 8 – (a) [Bmim]PF_6 decomposition under microwave radiation. (b) X-ray diffraction of the synthesized A_2SiF_6 (A = Li, Na, K, Rb, and Cs). Reproduced with permission from Ref. [71], copyright 2018, Wiley.

fluoride materials using an ionic liquid in the absence of HF. However, this study did not report on Mn^{4+}-activated fluorides.

4.3. *Ionothermal reaction using ionic liquid*

Recently, the synthesis of Na_2SiF_6 through an ionothermal reaction using an ionic liquid, 1-butyl-3-methylimidazolium tetrafluoroborate, without the use of toxic HF, was reported [77]. An ionothermal reaction is a method that uses an ionic liquid as the solvent, similar to the role of water in a hydrothermal reaction [78]. The red-emitting Mn^{4+}-activated Na_2SiF_6 phosphor was synthesized using Na_2SiF_6 with a low concentration of a HF solution. Fig. 9a shows a schematic diagram of the ionic liquid synthesis method for the host Na_2SiF_6. [Bmim]BF_4 consists of an organic cation ($Bmim^+$) and an anion (BF_4^-). During the ionothermal reaction, BF_4^- releases F^- that is used to form Na_2SiF_6. The equation below presents the formation mechanism of Na_2SiF_6 (Eqn (7)):

$$2NaBr(s) + Si(OCH_3)_4(l) + 6[Bmim]BF_4(l) \rightarrow Na_2SiF_6 + 2Br^-(aq) + 4(OCH_3)^-(aq) + 6BF_3(g) + 6[Bmim]^+(aq) \quad (7)$$

Fig. 9b displays the incorporation of $[MnF_6]^{2-}$ in $Na_2Si_{1-x}Mn_xF_6$ (x = 0.007, 0.100, and 0.200) performed in a 6 M HF solution (10 wt.% of HF). The XRD patterns of the synthesized $Na_2Si_{1-x}Mn_xF_6$ (x = 0.007, 0.100, and 0.200) match well with the powder diffraction file of Na_2SiF_6 without impurity peaks (Fig. 9c). The PL excitation (PLE) and PL spectra (λ_{ex} = 460 nm)

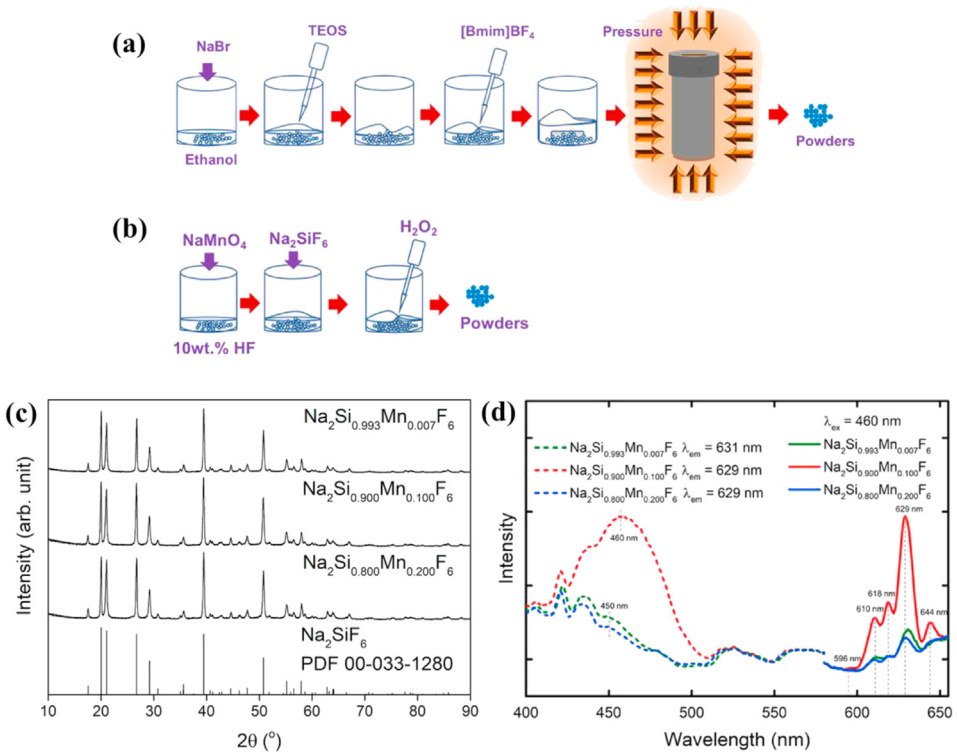

Fig. 9 – (a) Schematic diagram of the processes to synthesize Na_2SiF_6 using the ionic liquid, [Bmim]BF_4. (b) Synthesis process of $Na_2Si_{1-x}Mn_xF_6$ in a 6 M HF solution. (c) X-ray diffraction patterns and (d) photoluminesence spectra of $Na_2Si_{1-x}Mn_xF_6$ (x = 0.007, 0.100 and 0.200). Reproduced with permission from Ref. [77], copyright 2020, Elsevier.

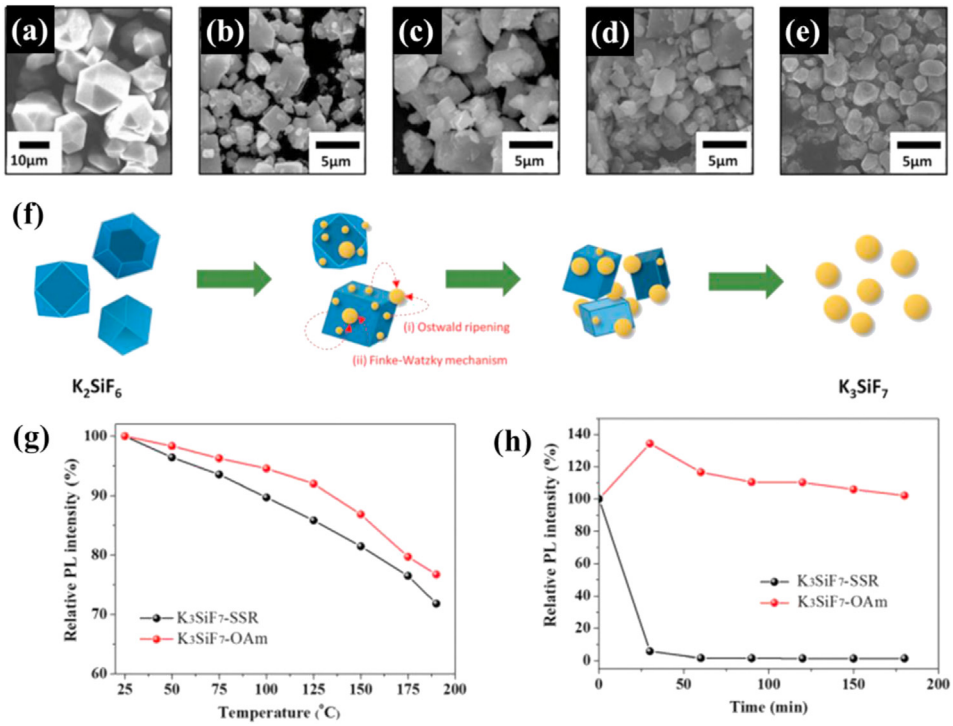

Fig. 10 – SEM images of K_3SiF_7:Mn^{4+} synthesized using oleylamine with reaction times of (a) 0 min, (b) 30 min, (c) 60 min, (d) 90 min, and (e) 120 min. (f) Schematic illustration of the shape evolution of K_3SiF_7:Mn^{4+} synthesized using oleylamine. Relative PL intensity of K_3SiF_7:Mn^{4+} phosphors as a function of (g) temperature and (h) exposure time under 85 °C/85% relative humidity. Reproduced with permission from Ref. [83], copyright 2019, The Royal Society of Chemistry.

of $Na_2Si_{1-x}Mn_xF_6$ (x = 0.007, 0.100, and 0.200) are shown in Fig. 9d, with the maximum intensity of the PLE and PL spectra at x = 0.100. The five emission peaks indicated in Fig. 9d at 596 nm, 610 nm, 618 nm, 629 nm, and 644 nm correspond to $\nu 3$ (tf_{1u}), $\nu 6$ (t_{2u}), ZPL, $\nu 6$ (t_{2u}), and $\nu 3$ (t_{1u}) vibronic modes of Mn^{4+}, respectively [17,20,22,23]. However, $Na_2Si_{1-x}Mn_xF_6$ has seven peaks in the range of 590–650 nm, which correspond to the ν_3 (t_{1u}), ν_4 (t_{1u}), ν_6 (t_{2u}), ZPL, ν_6 (t_{2u}), ν_4 (t_{1u}), and ν_3 (t_{1u}) vibronic modes according to previous studies [17,20,22,23]. Two peaks related to anti-Stokes (~605 nm) and Stokes (~631 nm) components of the ν_4 (t_{1u}) vibronic modes are missing in this result, which is attributed to the low concentration of HF (6 M). This low concentration of HF may not provide sufficient F^- to prevent the reduction or oxidation of Mn^{4+} during the incorporation of $[MnF_6]^{2-}$ into Na_2SiF_6. Although this work presents the use of an ionic liquid to synthesize Mn^{4+} activated fluoride, a low concentration of HF is needed for the incorporation of $[MnF_6]^{2-}$ into Na_2SiF_6, which also results in the missing emission peaks.

4.4. *Other methods using commercial K_2MnF_6*

Because of the increasing interest in sharp red-emitting phosphors, K_2MnF_6 is now produced commercially. This is an important precursor for the synthesis of Mn^{4+}-doped fluoride phosphors. Recently, researchers have investigated HF-free methods using commercial K_2MnF_6. The hosts have been synthesized using the HF-free method and then combined with K_2MnF_6 (commercially obtained or locally produced) to substitute Mn^{4+} ions into the host. Here, we introduce methods based on this process to expand on our discussion of HF-free methods. Xie et al. introduced a HF-free method using NH_4F/HCl instead of HF to produce A_2XF_6:Mn^{4+} phosphors (A = K, Na, Rb, and Cs; X = Si, Ge, and Ti) [79,80]. NH_4F and AF contribute sufficient F^- ions for the reaction, and HCl forms an acidic condition. Among these compositions, K_2GeF_6:Mn^{4+} has a high internal and external QE of 94% and 66%, respectively [79]. The Li_2SiF_6:Mn^{4+} phosphor was synthesized using high-pressure synthesis [81], and the ball-milling process combined with a solid-state method was investigated for the synthesis of K_3MnOF_7:Mn^{4+} [82]. The host, K_3MoOF_7, which was prepared from a mixture of MoO_3 with an excess of KHF_2, was obtained using the solid-state method. The K_3MoOF_7:Mn^{4+} phosphor was synthesized via a ball-milling process using the prepared K_3MoOF_7 host and K_2MnF_6. Lee et al. synthesized K_3SiF_7:Mn^{4+} phosphors from K_2SiF_6:Mn^{4+} phosphors using an organic solvent-assisted method [83]. The K_3SiF_7:Mn^{4+} phosphors were synthesized using a solid-state method and an organic solvent-assisted method from a mixture of K_2SiF_6, K_2MnF_6, and KHF_2. The solid-state method involved sintering at 400 °C for 7 h under a reduced atmosphere (75% N_2/25% H_2) in a tube furnace. In the organic solvent-assisted method, K_2SiF_6:Mn^{4+} phosphor was used as a precursor instead of K_2SiF_6 and K_2MnF_6. The mixture was placed in an organic solvent [oleic acid (OA), oleylamine (OAm), and trioctylphosphine oxide (TOPO)], and the resultant mixture was heated to 225 °C for 2 h in air. While the K_3SiF_7:Mn^{4+} phosphor was synthesized using OAm and TOPO, in contrast, the K_2SiF_6:Mn^{4+} phosphor was produced using OA, which means that the reaction had not progressed. The

Table 2 – Summary of synthesis methods without HF for Mn^{4+}-doped fluoride phosphors.

Methods	Reductant for Mn^{4+} ions	Advantage	Disadvantage	Host	Reference
Hydrothermal method	Low toxicity acid and KHF_2	• Use of a low toxicity acid	• Necessity of high temperature and pressure in synthesis • Necessary to improve quantum efficiency	K_2SiF_6	[69]
Microwave synthesis	Ionic liquid	• Use of low toxicity precursors • Short reaction times • High product yield	• Small particle sizes of the phosphors	A_2SiF_6 (A = Li, Na, K, Rb, and Cs)	[71]
Ionothermal reaction	Ionic liquid	• Use of low toxicity precursors • Synthesis of various compositions • High product yield	• Necessity of high temperature in synthesis • Small particle sizes of the phosphor	Na_2SiF_6	[77]
Co-precipitation	Low toxicity acid with commercial K_2MnF_6	• Use of low toxicity precursors • Does not require high temperatures • Synthesis of various compositions • More cost-effective than other methods • Products with high quantum efficiency	• Difficult to control the particle distribution depending on compositions	A_2XF_6 hexafluoride compositions	[79,80]
Solid-state method	Ball-milling, high pressure, or hydrogen gas with commercial K_2MnF_6	• Use of low toxicity precursors • Able to synthesize oxyfluoride compositions	• Necessity of high temperature in synthesis • Preparation under an argon gas atmosphere	Li_2SiF_6 K_3MoOF_7 K_3SiF_7	[81,82]
Organic-assisted solvent method	KHF_2 with commercial K_2MnF_6	• Products with high stability	• Necessity of high temperature in synthesis • Necessary to prepare K_2SiF_6	K_3SiF_7	[83]

reaction between the organic solvents and K_2SiF_6 (KHF_2) was confirmed using Fourier transform-infrared spectroscopy. Fig. 10a–e displays the shape evolution of the K_3SiF_7:Mn^{4+} phosphor with reaction time in the organic-assisted solvent method. Small particles of K_3SiF_7:Mn^{4+} were grown on the surface and the edge of K_2SiF_6. The growth of K_3SiF_7:Mn^{4+} nuclei occurred in two ways—Ostwald ripening and autocatalytic growth based on a Finke–Watzky two-step mechanism. Fig. 10f presents a schematic diagram of this process. K_3SiF_7:Mn^{4+} phosphors were prepared using an organic-assisted solvent method and a solid-state method, respectively (designated K_3SiF_7-OAm and K_3SiF_7-SSR). The thermal stability of these phosphors was investigated (Fig. 10g, h). K_3SiF_7-OAm exhibited better thermal stability than K_3SiF_7-SSR, even under high temperature and humidity conditions (85 °C/85% relative humidity). This is because of the residual OAm acting as a buffer layer to prevent a reaction with water on surface of the phosphor.

In this section, we presented various methods for the preparation of Mn^{4+}-doped fluoride phosphor without the use of HF. These are summarized in Table 2. Although these methods still have limitations with regard to the optical properties of the phosphors, they have shown the possibility of synthesizing fluoride phosphors without the use of HF.

5. Conclusions and perspectives

Mn^{4+}-doped fluoride red phosphors with narrow red emission peaks have been rapidly developed for high-quality LEDs. Since the first success of the etching method with Si wafers, various synthesis methods have been investigated in recent years. In this review, we discussed the synthesis methods that focus on the use of HF. Methods that make use of HF, such as etching, hydrothermal, and co-precipitation, have been reported for various fluoride compounds. In particular, the co-precipitation method has been applied for mass production, owing to its cost-efficiency and safety compared to other methods. Furthermore, in an effort to avoid the use of toxic HF, several HF-free methods using low toxicity acids or ionic liquids have been studied. HF reacts with F^- ions, which are key elements of the host materials, and prohibits oxidation and hydrolysis of F. Therefore, the synthesis requires highly acidic environments and excessive F^- ions. These HF-free methods are aimed to obtain similar optical properties of the phosphor compared with those obtained using HF-based methods. Because the optical properties of Mn^{4+}-doped phosphors are influenced by the reduction of Mn sources, it is difficult to obtain a material with reducing ability to replace HF. In addition to the aforementioned HF-free methods, a mechanochemical method or high-power ball-milling method, which has been proven to synthesize fluoride hosts, can be developed. Moreover, as displays and lighting techniques advance, there is a need for red-emitting phosphors that can be applied to high-power applications. The stability of phosphors is one of the crucial factors for high-power LEDs or laser diode applications; thus, enhancing the chemical/thermal stability is critical. Various coating methods or surface modifications of phosphors have been studied to enhance the stability with respect to moisture and heat exposure. These methods serve as additional processes after synthesis; thus, the surface of the phosphors will need to be modified simultaneously with phase synthesis to improve the stability. Finally, it is expected that an eco-friendly HF-free method will be developed for mass production, based on the methods mentioned here, and will result in the synthesis of phosphors that exhibit good optical performance.

Declaration of Competing Interest

The authors declare that they have no known competing financial interests or personal relationships that could have appeared to influence the work reported in this paper.

Acknowledgments

This work was financially supported by the National Research Foundation of Korea (NRF), South Korea grant funded by the Korean government (MSIT) (NRF-2017R1A2B3011967 and NRF-2018R1A5A1025224). This work was also performed under the auspices of the U.S. Department of Energy, USA by Lawrence Livermore National Laboratory under Contract DE-AC52-07NA27344.

REFERENCES

[1] McKittrick J, Shea-Rohwer LE. Down conversion materials for solid-state lighting. J Am Ceram Soc 2014;97(5):1327–52.
[2] Oh JH, Eo YJ, Yoon HC, Huh Y-D, Do YR. Evaluation of new color metrics: guidelines for developing narrow-band red phosphors for WLEDs. J Mater Chem C 2016;4(36):8326–48.
[3] Pust P, Weiler V, Hecht C, Tücks A, Wochnik AS, Henß A-K, et al. Narrow-band red-emitting $Sr[LiAl_3N_4]:Eu^{2+}$ as a next-generation LED-phosphor material. Nat Mater 2014;13(9):891–6.
[4] Wang Z, Chu I-H, Zhou F, Ong SP. Electronic structure descriptor for the discovery of narrow-band red-emitting phosphors. Chem Mater 2016;28(11):4024–31.
[5] Hoerder GJ, Seibald M, Baumann D, Schröder T, Peschke S, Schmid PC, et al. $Sr[Li_2Al_2O_2N_2]:Eu^{2+}$—a high performance red phosphor to brighten the future. Nat Commun 2019;10(1):1–9.
[6] Lin CC, Meijerink A, Liu RS. Critical red components for next-generation white LEDs. J Phys Chem Lett 2016;7(3):495–503.
[7] Protesescu L, Yakunin S, Bodnarchuk MI, Krieg F, Caputo R, Hendon CH, et al. Nanocrystals of cesium lead halide perovskites ($CsPbX_3$, X= Cl, Br, and I): novel optoelectronic materials showing bright emission with wide color gamut. Nano Lett 2015;15(6):3692–6.
[8] Adachi S. Photoluminescence spectra and modeling analyses of Mn^{4+}-activated fluoride phosphors: a review. J Lumin 2018;197:119–30.
[9] Sijbom HF, Verstraete R, Joos JJ, Poelman D, Smet PF. $K_2SiF_6:Mn^{4+}$ as a red phosphor for displays and warm-white LEDs: a review of properties and perspectives. Opt Mater Express 2017;7(9):3332–65.
[10] Zhou Q, Dolgov L, Srivastava AM, Zhou L, Wang Z, Shi J, et al. Mn^{2+} and Mn^{4+} red phosphors: synthesis, luminescence and

applications in WLEDs. A review. J Mater Chem C 2018;6(11):2652–71.
[11] Tanabe Y, Sugano S. On the absorption spectra of complex ions II. J Phys Soc Jpn 1954;9(5):766–79.
[12] Cao R, Zhang F, Cao C, Yu X, Liang A, Guo S, et al. Synthesis and luminescence properties of $CaAl_2O_4:Mn^{4+}$ phosphor. Opt Mater 2014;38:53–6.
[13] Li Y, Qi S, Li P, Wang Z. Research progress of Mn doped phosphors. RSC Adv 2017;7(61):38318–34.
[14] Adachi S, Takahashi T. Direct synthesis and properties of $K_2SiF_6:Mn^{4+}$ phosphor by wet chemical etching of Si wafer. J Appl Phys 2008;104(2):023512.
[15] Xu YK, Adachi S. Properties of $Na_2SiF_6:Mn^{4+}$ and $Na_2GeF_6:Mn^{4+}$ red phosphors synthesized by wet chemical etching. J Appl Phys 2009;105(1):013525.
[16] Lv L, Jiang X, Huang S, Chen X, Pan Y. The formation mechanism, improved photoluminescence and LED applications of red phosphor $K_2SiF_6:Mn^{4+}$. J Mater Chem C 2014;2(20):3879–84.
[17] Zhu H, Lin CC, Luo W, Shu S, Liu Z, Liu Y, et al. Highly efficient non-rare-earth red emitting phosphor for warm white light-emitting diodes. Nat Commun 2014;5(1–10):4312.
[18] Wei L-L, Lin CC, Fang M-H, Brik MG, Hu S-F, Jiao H, et al. A low-temperature co-precipitation approach to synthesize fluoride phosphors $K_2MF_6:Mn^{4+}$ (M= Ge, Si) for white LED applications. J Mater Chem C 2015;3(8):1655–60.
[19] Tang F, Su Z, Ye H, Wang M, Lan X, Phillips DL, et al. A set of manganese ion activated fluoride phosphors ($A_2BF_6:Mn^{4+}$, A = K, Na, B= Si, Ge, Ti): synthesis below 0°C and efficient room-temperature photoluminescence. J Mater Chem C 2016;4(40):9561–8.
[20] Wang Z, Liu Y, Zhou Y, Zhou Q, Tan H, Zhang Q, et al. Red-emitting phosphors $Na_2XF_6:Mn^{4+}$ (X= Si, Ge, Ti) with high colour-purity for warm white-light-emitting diodes. RSC Adv 2015;5(72):58136–40.
[21] Kasa R, Adachi S. Red and deep red emissions from cubic $K_2SiF_6:Mn^{4+}$ and hexagonal K_2MnF_6 synthesized in HF/$KMnO_4$/KHF_2/Si solutions. J Electrochem Soc 2012;159(4):J89–95.
[22] Nguyen H-D, Lin CC, Fang M-H, Liu R-S. Synthesis of $Na_2SiF_6:Mn^{4+}$ red phosphors for white LED applications by co-precipitation. J Mater Chem C 2014;2(48):10268–72.
[23] Lang T-C, Han T, Peng L-L, Tu M-J. Luminescence properties of $Na_2SiF_6:Mn^{4+}$ red phosphors for high colour-rendering white LED applications synthesized via a simple exothermic reduction reaction. Materials Chemistry Frontiers 2017;1(5):928–32.
[24] Adachi S. Crystal-field and Racah parameters of Mn^{4+} ion in red and deep red-emitting phosphors: fluoride versus oxide phosphor. J Lumin 2020;218:116829.
[25] Yi X, Li R, Zhu H, Gao J, You W, Gong Z, et al. $K_2NaAlF_6:Mn^{4+}$ red phosphor: room-temperature synthesis and electronic/vibronic structures. J Mater Chem C 2018;6(8):2069–76.
[26] Senden T, Geitenbeek R, Meijerink A. Co-precipitation synthesis and optical properties of Mn^{4+}-doped hexafluoroaluminate w-LED phosphors. Materials 2017;10(11):1322.
[27] Takahashi T, Adachi S. Mn^{4+}-activated red photoluminescence in K_2SiF_6 phosphor. J Electrochem Soc 2008;155(12):E183–8.
[28] Adachi S, Takahashi T. Direct synthesis of $K_2SiF_6:Mn^{4+}$ red phosphor from crushed quartz schist by wet chemical etching. Electrochem Solid State Lett 2009;12(2):J20–3.
[29] Takahashi T, Adachi S. Synthesis of $K_2SiF_6:Mn^{4+}$ red phosphor from silica glasses by wet chemical etching in HF/$KMnO_4$ solution. Electrochem Solid State Lett 2009;12(8):J69–71.
[30] Nakamura T, Yuan Z, Adachi S. Micronization of red-emitting $K_2SiF_6:Mn^{4+}$ phosphor by pulsed laser irradiation in liquid. Appl Surf Sci 2014;320:514–8.
[31] Chodos S, Black A, Flint C. Vibronic spectra and lattice dynamics of Cs_2MnF_6 and $A^{12}M^{IV}F_6:MnF_6^{2-}$. J Chem Phys 1976;65(11):4816–24.
[32] Setlur AA, Radkov EV, Henderson CS, Her J-H, Srivastava AM, Karkada N, et al. Energy-efficient, high-color-rendering LED lamps using oxyfluoride and fluoride phosphors. Chem Mater 2010;22(13):4076–82.
[33] Gao X, Song Y, Liu G, Dong X, Wang J, Yu W. $BaTiF_6:Mn^{4+}$ bifunctional microstructures with photoluminescence and photocatalysis: hydrothermal synthesis and controlled morphology. CrystEngComm 2016;18(31):5842–51.
[34] Zhu Y, Huang L, Zou R, Zhang J, Yu J, Wu M, et al. Hydrothermal synthesis, morphology and photoluminescent properties of an Mn^{4+}-doped novel red fluoride phosphor elpasolite K_2LiAlF_6. J Mater Chem C 2016;4(24):5690–5.
[35] Cheng H, Song Y, Liu G, Li D, Dong X, Wang J, et al. Hydrothermal synthesis of narrow-band red emitting $K_2NaAlF_6:Mn^{4+}$ phosphor for warm-white LED applications. RSC Adv 2017;7(72):45834–42.
[36] Hong F, Cheng H, Liu G, Dong X, Yu W, Wang J. Controlled morphology, improved photoluminescent properties, and application of an efficient non-rare earth deep red-emitting phosphor. Inorg Chem 2018;57(16):9892–901.
[37] Jiang C, Brik MG, Srivastava AM, Li L, Peng M. Significantly conquering moisture-induced luminescence quenching of red line-emitting phosphor $Rb_2SnF_6:Mn^{4+}$ through $H_2C_2O_4$ triggered particle surface reduction for blue converted warm white light-emitting diodes. J Mater Chem C 2019;7(2):247–55.
[38] Xi L, Pan Y, Chen X, Huang S, Wu M. Optimized photoluminescence of red phosphor $Na_2SnF_6:Mn^{4+}$ as red phosphor in the application in "warm" white LED s. J Am Ceram Soc 2017;100(5):2005–15.
[39] Jia H, Cao L, Wei Y, Wang H, Xiao H, Li G, et al. A narrow-band red-emitting $K_2LiGaF_6:Mn^{4+}$ phosphor with octahedral morphology: luminescent properties, growth mechanisms, and applications. J Alloys Compd 2018;738:307–16.
[40] Hong F, Cheng H, Song C, Liu G, Yu W, Wang J, et al. Novel polygonal structure Mn^{4+} activated In^{3+}-based Elpasolite-type hexafluorides red phosphor for warm white light-emitting diodes (WLEDs). Dalton Trans 2019;48(4):1376–85.
[41] Sekiguchi D, Nara J-i, Adachi S. Photoluminescence and Raman scattering spectroscopies of $BaSiF_6:Mn^{4+}$ red phosphor. J Appl Phys 2013;113(18):183516.
[42] Lin H, Hu T, Huang Q, Cheng Y, Wang B, Xu J, et al. Non-rare-earth $K_2XF_7:Mn^{4+}$ (X= Ta, Nb): a highly-efficient narrow-band red phosphor enabling the application in wide-color-gamut LCD. Laser Photon Rev 2017;11(6):1700148.
[43] Kumada N, Yanagida S, Takei T, Hong B. Hydrothermal synthesis and crystal structure of new red phosphors, $KNaMF_7:Mn^{4+}$ (M: Nb, Ta). Mater Res Bull 2019;115:170–5.
[44] Zhou Y, Zhang S, Wang X, Jiao H. Structure and luminescence properties of Mn^{4+}-activated $K_3TaO_2F_4$ red phosphor for white LEDs. Inorg Chem 2019;58(7):4412–9.
[45] Liang Z, Yang Z, Tang H, Guo J, Yang Z, Zhou Q, et al. Synthesis, luminescence properties of a novel oxyfluoride red phosphor $BaTiOF_4:Mn^{4+}$ for LED backlighting. Opt Mater 2019;90:89–94.
[46] Zhou Q, Zhou Y, Liu Y, Luo L, Wang Z, Peng J, et al. A new red phosphor $BaGeF_6:Mn^{4+}$: hydrothermal synthesis, photoluminescence properties, and its application in warm white LED devices. J Mater Chem C 2015;3(13):3055–9.
[47] Li Q, Luo R, Feng L, Dong C, Ning Z, Liu M, et al. A novel red phosphor of $BaGe_{(1-x)}Ti_xF_6:Mn^{4+}$ solid solution: facile hydrothermal controlled synthesis, microstructures and

luminescent properties. J Mater Chem C 2019;7(36):11265–75.
[48] Lv L, Jiang X, Pan Y, Liu G, Huang S. Luminescence properties and thermal stability of a red phosphor $ZnSiF_6{\cdot}6H_2O{:}Mn^{4+}$ synthesized by the one-step hydrothermal method. J Lumin 2014;152:214–7.
[49] Pan Y, Chen Z, Jiang X, Huang S, Wu M. A facile route to $BaSiF_6{:}Mn^{4+}$ phosphor with intense red emission and its humidity stability. J Am Ceram Soc 2016;99(9):3008–14.
[50] Zhou Q, Zhou Y, Lu F, Liu Y, Wang Q, Luo L, et al. Mn^{4+}-activated $BaSiF_6$ red phosphor: hydrothermal synthesis and dependence of its luminescent properties on reaction conditions. Mater Chem Phys 2016;170:32–7.
[51] Jia H, Duan Y, Gao J, Yuan X, Wang H, Li G. Enhanced red emission for $BaSiF_6{:}Mn^{4+}$ hexagonal nanorod phosphor via using spherical silica. Mater Lett 2018;223:163–5.
[52] Jiang X, Pan Y, Huang S, Chen X, Wang J, Liu G. Hydrothermal synthesis and photoluminescence properties of red phosphor $BaSiF_6{:}Mn^{4+}$ for LED applications. J Mater Chem C 2014;2(13):2301–6.
[53] Mo G, Wang W, Wang K, Wen G, Zhu M, Wang J. Deep red $BaTiF_4{:}Mn^{4+}$ phosphor: synthesis, optical properties and application for warm WLED devices. J Mater Sci Mater Electron 2017;28(11):8155–9.
[54] Cai P, Wang X, Seo HJ. Excitation power dependent optical temperature behaviors in Mn^{4+} doped oxyfluoride $Na_2WO_2F_4$. Phys Chem Chem Phys 2018;2(3):2028–35.
[55] Xi L, Pan Y, Zhu M, Lian H, Lin J. Abnormal site occupancy and high performance in warm WLEDs of a novel red phosphor, $NaHF_2{:}Mn^{4+}$, synthesized at room temperature. Dalton Trans 2017;46(40):13835–44.
[56] Wang L, Song E, Zhou Y, Deng T, Ye S, Zhang Q. Synthesis and warm-white LED applications of an efficient narrow-band red emitting phosphor, $Rb_2ZrF_6{:}Mn^{4+}$. J Mater Chem C 2017;5(29):7253–61.
[57] Deng T, Song E, Zhou Y, Wang L, Ye S, Zhang Q. Stable narrowband red phosphor $K_3GaF_6{:}Mn^{4+}$ derived from hydrous $K_2GaF_5(H_2O)$ and K_2MnF_6. J Mater Chem C 2017;5(37):9588–96.
[58] Zhu M, Pan Y, Xi L, Lian H, Lin J. Design, preparation, and optimized luminescence of a dodec-fluoride phosphor $Li_3Na_3Al_2F_{12}{:}Mn^{4+}$ for warm WLED applications. J Mater Chem C 2017;5(39):10241–50.
[59] Liu Y, Gao G, Huang L, Zhu Y, Zhang X, Yu J, et al. Co-precipitation synthesis and photoluminescence properties of $BaTiF_6{:}Mn^{4+}$: an efficient red phosphor for warm white LEDs. J Mater Chem C 2018;6(1):127–33.
[60] Hu T, Lin H, Lin F, Gao Y, Cheng Y, Xu J, et al. Narrow-band red-emitting $KZnF_3{:}Mn^{4+}$ fluoroperovskites: insights into electronic/vibronic transition and thermal quenching behavior. J Mater Chem C 2018;6(40):10845–54.
[61] Lian H, Huang Q, Chen Y, Li K, Liang S, Shang M, et al. Resonance emission enhancement (REE) for narrow band red-emitting $A_2GeF_6{:}Mn^{4+}$ (A= Na, K, Rb, Cs) phosphors synthesized via a precipitation–cation exchange route. Inorg Chem 2017;56(19):11900–10.
[62] Wang Z, Yang Z, Yang Z, Wei Q, Zhou Q, Ma L, et al. Red phosphor $Rb_2NbOF_5{:}Mn^{4+}$ for warm white light-emitting diodes with a high color-rendering index. Inorg Chem 2018;58(1):456–61.
[63] Ming H, Liu S, Liu L, Peng J, Fu J, Du F, et al. Highly regular, uniform $K_3ScF_6{:}Mn^{4+}$ phosphors: facile synthesis, microstructures, photoluminescence properties, and application in light-emitting diode devices. ACS Appl Mater Interfaces 2018;10(23):19783–95.
[64] Zhou W, Fang M-H, Lian S, Liu R-S. Ultrafast self-crystallization of high-external-quantum-efficient fluoride phosphors for warm white light-emitting diodes. ACS Appl Mater Interfaces 2018;10(21):17508–11.
[65] Xu H, Hong F, Chen Z, Nan S, Wang Y, Liu G, et al. Green route, room-temperature synthesis and luminescence properties of a non-rare-earth doping Zn^{2+} based narrow-band red phosphor for WLEDs. J Lumin 2019;216:116695.
[66] Zhang J, Liu L, He S, Peng J, Du F, Yang F, et al. Cs_2MnF_6 red phosphor with ultrahigh absorption efficiency. Inorg Chem 2019;58(22):15207–15.
[67] Zhou W, Wang R-H, Yin L, Chen J, Su C, Xing X, et al. Alcohol-guided growth of two-dimensional narrow-band red-emitting $K_2TiF_6{:}\ Mn^{4+}$ for white-light-emitting diodes. ACS Appl Mater Interfaces 2019;11(22):20143–9.
[68] Zhang C, Han T, Cao S, Cheng X, Zhang J. Mn^{4+}-doped fluoride phosphors rapidly synthesized by ball milling. Opt Mater Express 2018;8(1):73–81.
[69] Huang L, Zhu Y, Zhang X, Zou R, Pan F, Wang J, et al. HF-free hydrothermal route for synthesis of highly efficient narrow-band red emitting phosphor $K_2Si_{1-x}F_6{:}xMn^{4+}$ for warm white light-emitting diodes. Chem Mater 2016;28(5):1495–502.
[70] Liao C, Cao R, Ma Z, Li Y, Dong G, Sharafudeen KN, et al. Synthesis of $K_2SiF_6{:}Mn^{4+}$ phosphor from SiO_2 powders via redox reaction in $HF/KMnO_4$ solution and their application in warm-white LED. J Am Ceram Soc 2013;96(11):3552–6.
[71] Olchowka J, Suta M, Wickleder C. Green synthesis of A_2SiF_6 (A= Li–Cs) nanoparticles using ionic liquids as solvents and as fluorine sources: a simple approach without HF. Chemistry–A European Journal 2017;23(50):12092–5.
[72] Lorbeer C, Mudring AV. Ionic liquid-assisted route to nanocrystalline single-phase phosphors for white light-emitting diodes. ChemSusChem 2013;6(12):2382–7.
[73] Olchowka J, Hagemann H, Delgado T, Wickleder C. The influence of ionothermal synthesis using $BmimBF_4$ as a solvent on nanophosphor $BaFBr{:}Eu^{2+}$ photoluminescence. Nanoscale 2018;10(42):19706–10.
[74] Terraschke H, Olchowka J, Geringer E, Rodrigues AV, Wickleder C. Facile ionic liquid-assisted strategy for direct precipitation of Eu^{2+}-activated nanophosphors under ambient conditions. Small 2018;14(17):1703707.
[75] Xue H, Verma R, Jean'ne MS. Review of ionic liquids with fluorine-containing anions. J Fluor Chem 2006;127(2):159–76.
[76] Freudenmann D, Wolf S, Wolff M, Feldmann C. Ionic liquids: new perspectives for inorganic synthesis? Angew Chem Int Ed 2011;50(47):11050–60.
[77] Ha J, Novitskaya E, Lam N, Sanchez M, Kim YH, Li Z, et al. Synthesis of Mn^{4+} activated Na_2SiF_6 red-emitting phosphors using an ionic liquid. J Lumin 2020;218:116835.
[78] Morris RE. Ionothermal synthesis—ionic liquids as functional solvents in the preparation of crystalline materials. Chem Commun 2009;(21):2990–8.
[79] Luo X, Hou Z, Zhou T, Xie RJ. A universal HF-free synthetic method to highly efficient narrow-band red-emitting $A_2XF_6{:}Mn^{4+}$ (A = K, Na, Rb, Cs; X = Si, Ge, Ti) phosphors. J Am Ceram Soc 2020;103(2):1018–26.
[80] Hou Z, Tang X, Luo X, Zhou T, Zhang L, Xie R-J. A green synthetic route to the highly efficient $K_2SiF_6{:}Mn_{4+}$ narrow-band red phosphor for warm white light-emitting diodes. J Mater Chem C 2018;6(11):2741–6.
[81] Stoll C, Bandemehr J, Kraus F, Seibald M, Baumann D, Schmidberger MJ, et al. HF-free synthesis of $Li_2SiF_6{:}Mn^{4+}$: a red-emitting phosphor. Inorg Chem 2019;58(9):5518–23.
[82] Stoll C, Seibald M, Baumann D, Huppertz H. HF-Free solid-state synthesis of the oxyfluoride phosphor $K_3MoOF_7{:}Mn^{4+}$. Eur J Inorg Chem 2019;29:3383–8.
[83] Noh M, Yoon DH, Kim CH, Lee SJ. Organic solvent-assisted synthesis of the $K_3SiF_7{:}Mn^{4+}$ red phosphor with improved morphology and stability. J Mater Chem C 2019;7(47):15014–20.